

Evgeni Fedorovich\* and Robert Conzemius  
School of Meteorology, University of Oklahoma, Norman, Oklahoma

## 1. INTRODUCTION

Early stages in the development of the inversion-capped atmospheric convective boundary layer (CBL) were studied by means of numerical large eddy simulation (LES) in conjunction with data from the University of Karlsruhe (UniKa) wind tunnel model of the atmospheric CBL (Fedorovich *et al.* 1996, 2001). The LES experiments were conducted for two CBL flow types. The first investigated type was the spatially evolving quasi-stationary CBL modeled in the wind tunnel. The second type was the nonsteady, horizontally quasi-homogeneous CBL in a periodic domain. The latter CBL type is commonly considered in meteorological applications of LES. Thus, the dynamics of convective entrainment in a pure case of *spatial* CBL evolution was analyzed versus the entrainment dynamics in a pure case of CBL *temporal* development.

In the LES of atmospheric convection, (see, *e.g.* Nieuwstadt *et al.* 1993), convective motions are traditionally initiated by prescribing randomly distributed velocity and temperature fluctuations throughout an originally homogeneous flow region beneath the inversion. The subsequent development of convection passes through a transition phase, properties of which (in particular, the duration of transition) essentially depend on the depth of the perturbed layer and characteristics of the imposed fluctuations. In order to avoid an arbitrary choice for the initial perturbed layer depth, the resolved-scale temperature and/or velocity perturbations in the present study were generated only in the immediate vicinity of the underlying surface. The effects of magnitude and correlation of such perturbations on the stimulation of convection in shear-free and sheared clear boundary layers driven by surface buoyant forcing were systematically investigated.

## 2. LES TECHNIQUE EMPLOYED

Two versions of the LES code described in Nieuwstadt and Brost (1986) were employed in the conducted study. The first one, a modified version of the code, allowed introduction of inflow/outflow and lateral-wall boundary conditions (Fedorovich *et al.* 2001) in order to simulate the wind tunnel CBL. The second version was rather similar to the original version of the code, but used updated lower boundary conditions and a modified sponge layer at the CBL top. It was

employed for the simulation of the nonsteady CBL in a box-like domain with periodic lateral boundary conditions. In this version of the code, either the turbulence kinetic energy subgrid closure (also known as Deardorff closure, see Deardorff 1980) or the Smagorinsky subgrid closure (Lilly 1967) was used. The standard values of dimensionless constants were used in both closure models. The LES runs for the horizontally evolving CBL were conducted only with Deardorff closure.

## 3. EXPERIMENTAL SETUP

### 3.1 Horizontally evolving CBL

The UniKa wind tunnel is a close-circuit type facility, with a 10m×1.5m×1.5m test section (Rau and Plate 1995). It is specially designed for simulating the horizontally evolving, inversion-capped atmospheric CBL. The return section of the tunnel is subdivided into ten individually insulated and controlled layers. This allows preshaping of the velocity and temperature profiles at the inlet of the test section. A feedback control system enforces quasi-stationary conditions for the inflow. The test section floor is heated with a controlled energy input to produce a constant heat flux through the floor.

In the LES of the horizontally evolving (wind tunnel) CBL, the values of velocity components and temperature at the domain (test section) inlet were decomposed in two parts. The first part (the stationary part) was a steady value corresponding to the settings of the tunnel control system for each particular flow configuration. The second part represented a nonstationary fluctuating component of the inflow. These fluctuations were prescribed as normally distributed noncorrelated random values with a given variance. The simulations were performed on the 400×60×60 grid with uniform spacing in all directions.

### 3.2 Nonsteady CBL

A variety of convection initiation regimes in a linearly (*i.e.* with a height-constant buoyancy frequency) stratified atmosphere was considered. The regimes differed by the magnitude of the random resolved-scale vertical velocity and (potential) temperature perturbations prescribed in the first layer of grid cells adjacent to the surface. Both correlated and noncorrelated distributions of temperature and velocity were used for the initiation.

The simulations were performed in a rectangular domain  $X \times Y \times Z = 2560 \times 2560 \times 1600 \text{m}^3$  with  $128 \times 128 \times 80$  cubic grid cells. The kinematic heat flux through the

---

\* Corresponding author address: Evgeni Fedorovich, School of Meteorology, University of Oklahoma, 100 East Boyd, Norman, OK 73019-1013; e-mail: fedorovich@ou.edu

underlying surface was kept constant. In the experiments to be discussed below, its value was  $0.3\text{K}\cdot\text{m}^{-1}$  and the potential temperature gradient in the stably stratified atmosphere was taken equal to  $0.003\text{K}\cdot\text{m}^{-1}$ . The aerodynamic roughness length of the underlying surface was  $0.01\text{m}$ . The sponge layer with a sine-type damping occupied the upper 20% of the domain depth. The shear forcing was introduced through a single-component geostrophic wind. In the considered experiments, this wind was either constant and equal to  $20\text{m}\cdot\text{s}^{-1}$  throughout the whole domain (a barotropic case), or changing linearly with height from  $0\text{m}\cdot\text{s}^{-1}$  at the surface to  $20\text{m}\cdot\text{s}^{-1}$  at the domain top (a quasi-baroclinic case).

#### 4. SIMULATION RESULTS

##### 4.1 Horizontally evolving CBL

Substantial initial temperature and velocity fluctuations are typically present only in the two lower open-circuit layers of the tunnel. The magnitudes of temperature and velocity fluctuations in these layers can reach up to several tens of K and  $0.5\text{m}\cdot\text{s}^{-1}$ , respectively. Above the inversion, the magnitudes of the temperature and velocity fluctuations are considerably smaller. These estimates were used for setting the nonstationary components of the inlet velocity and temperature in the LES experiments. Numerical results closest to the measured data have been obtained for the case when only the lowest  $0.3\text{m}$ -deep portion of the LES inlet temperature field had prescribed random disturbances with rms of  $50\text{K}$  (TF case). The LES data for the TF case are compared with the wind tunnel data in Fig. 1. Different line and marker styles correspond to different locations: dashed-dotted line and stars to  $x=0.68\text{m}$ ; dashed-double-dotted line and crosses to  $x=2.33\text{m}$ ; solid line and squares to  $x=3.98\text{m}$ ; dashed line and triangles to  $x=5.63\text{m}$ ; and dotted line and diamonds to  $x=7.28\text{m}$ .

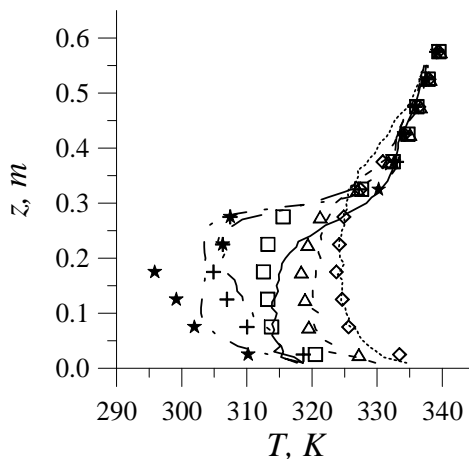


Figure 1. Temperature field evolution in the TF case.

Based on the temperature evolution pattern in Fig. 1, one may conclude that transition from the unstable

premixed layer to the convectively mixed layer happens over a comparatively short distance between  $x=2.33\text{m}$  and  $x=3.98\text{m}$ . Insufficient mixing at the early stages of convection (at  $x\leq 2.5\text{m}$ ) leads to accumulation of potential energy in the unstable two-layer fluid system composed of a hot layer underlying a pool of cooler and less buoyant air. This unstable system eventually overturns and the accumulated energy is transformed into kinetic energy of turbulent fluctuations that effectively mix up the under-inversion air. See the evolution pattern of the vertical velocity variance for the TF case in the upper plot of Fig. 2.

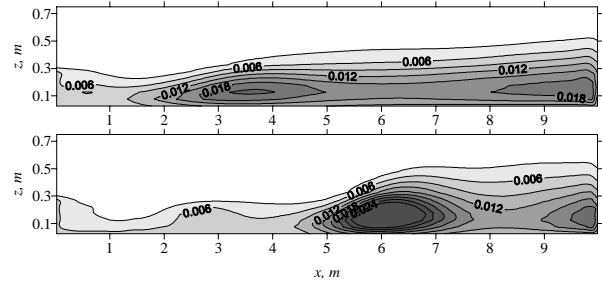


Figure 2. Horizontal evolution of  $\overline{w'^2}$  ( $\text{m}^2\cdot\text{s}^{-2}$ ) along the CBL in the TF (upper plot) and NF (lower plot) cases.

Next, we consider the LES results corresponding to the stationary inflow with no resolved-scale velocity and temperature fluctuations (NF case). Numerical results presented in the lower plot of Fig. 2 show that with such inflow conditions, the transition to a well-mixed CBL is substantially delayed compared to the TF case. Thus, in the numerically simulated flow without initial disturbances, the turbulence and mixing below the inversion develop much more slowly than in the flow with initial temperature disturbances. Such insufficient mixing leads to a substantial accumulation of potential energy in the aforementioned unstable two-layer fluid system that precedes the transition. The eventual release of energy in the transition zone has a form of a turbulence outbreak, which is clearly seen in the pattern of  $\overline{w'^2}$  for the NF case at  $5\text{m} < x < 7\text{m}$ . Downwind of the transition region, the vertical extension of the convectively mixed zone does not change significantly with distance and turbulence levels within this zone return to values smaller than those in the transition region.

##### 4.2 Nonsteady CBL

As a reference case for the evaluation of initial perturbation effects on the nonsteady CBL development we take the initiation regime in the shear-free CBL with rather large and noncorrelated temperature and vertical velocity fluctuations at the underlying surface. Their rms values were set equal to  $2\text{K}$  and to  $2\text{m}\cdot\text{s}^{-1}$ , respectively. This case, with the Deardorff (1980) subgrid model employed for the LES closure, will be referred to as NST2W2D.

Effects of correlated perturbations will be addressed separately in our presentation at the conference.

Simulated mean potential temperature, potential temperature variance, kinematic turbulent heat flux  $Q = \overline{w'\theta'}$ , and vertical velocity variance profiles at different stages of the CBL evolution in the NST2W2D case are displayed in Fig. 3. The shown statistics were obtained by spatial averaging over horizontal planes.

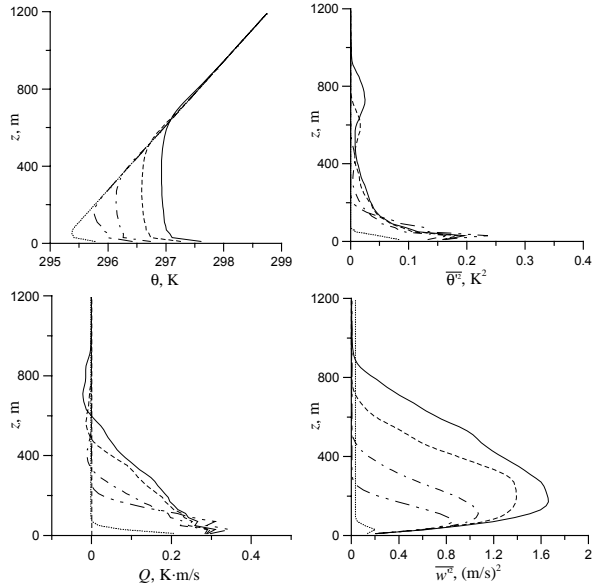


Figure 3. Evolution of mean potential temperature and turbulence statistics fields in the NST2W2D case. The lines correspond to the following times in the simulation:  $t=60s$  (dotted lines),  $t=300s$  (dashed-double-dotted lines),  $t=600s$  (dashed-dotted lines),  $t=1200s$  (dashed lines), and  $t=1800s$  (solid lines).

From the presented plots, one may conclude that in the case of large initial perturbations, the mixed-layer phase of the CBL development is achieved rather fast, within about 10-min time after the convection onset. Once this phase is achieved, the turbulence structure of the CBL develops in time in a self-similar manner.

The LES data indicate, however, that with very small initial temperature or/and vertical velocity disturbances, whose their rms values are set at the limit of computational precision in our experiments ( $\sim 10^{-7}K$  and/or  $\sim 10^{-7}m\cdot s^{-1}$ ), the CBL development occurs in a very different way. We found that in this case, which is referred to as NST-W-D case, drastic heat buildup occurs for some time in the almost quiescent (with a vanishingly weak turbulence) near-surface region of the flow as shown in Fig. 4. This heat buildup is followed by the explosive development of convection, resulting in large velocities that rapidly mix heat vertically, overcompensating for the specified heat flux at the surface. In a certain sense, this development is rather similar to the one in the horizontally evolving CBL with zero initial disturbances (section 4.1). The difference is that with no disturbances the resolved-scale convection in the nonsteady CBL is not initiated at all. The explosive development of convection in the NST-W-D case results, for a time, in excessive mixing so that

thermal gradients in the surface layer become insufficient to maintain the intensity of convection. A subsequent decrease in convection (not seen in the plots) occurs, followed by a secondary heat buildup at the surface, thus indicating a cyclic nature of the convection initiation. The magnitude of this cycle quickly decreases as a steady convection stage is reached.

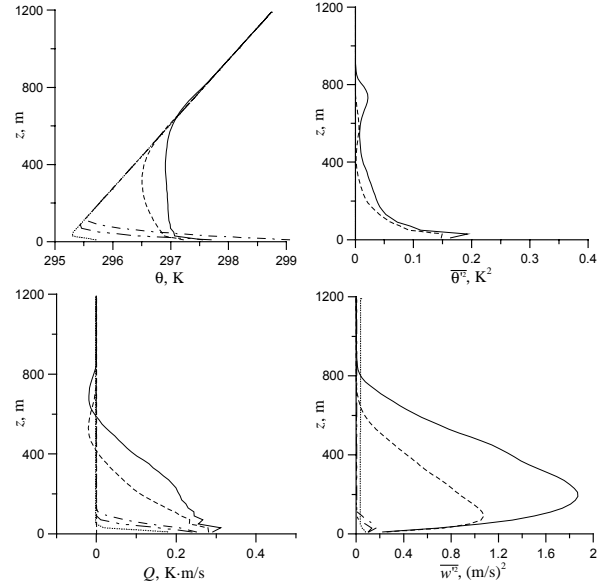


Figure 4. Evolution of the CBL structure in the NST-W-D case. For notation, see Fig. 3.

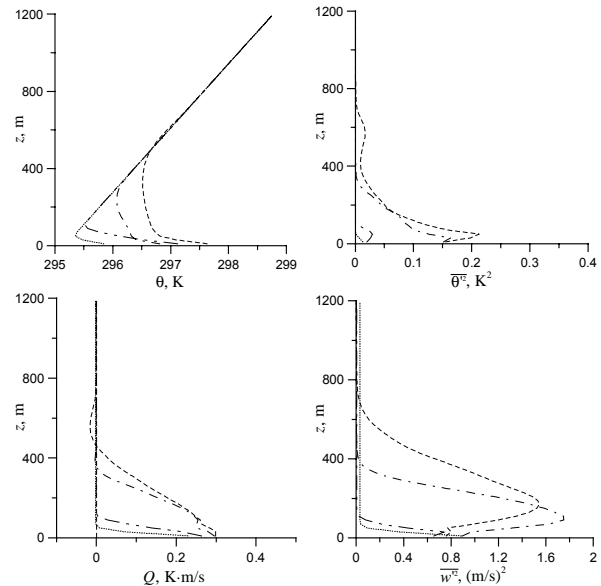


Figure 5. Evolution of the CBL structure in the GCT2W2D case. For notation, see Fig. 3.

The presence of height-constant  $20m\cdot s^{-1}$  geostrophic wind was found to substantially inhibit the initial stage of the CBL growth in the simulated flow case denoted as

GCT2W2D (the temperature and velocity perturbations in this case are the same as in the NST2W2D case). Such inhibition is clearly seen in the plots of flow statistics shown in Fig. 5. Apparently, the buoyantly driven vertical motions at the initial stages of convection are severely distorted by the surface shear in this case. As a result, the evolution of vertical mixing in the CBL is considerably slowed down compared to the shear-free case NST2W2D, see Fig. 3.

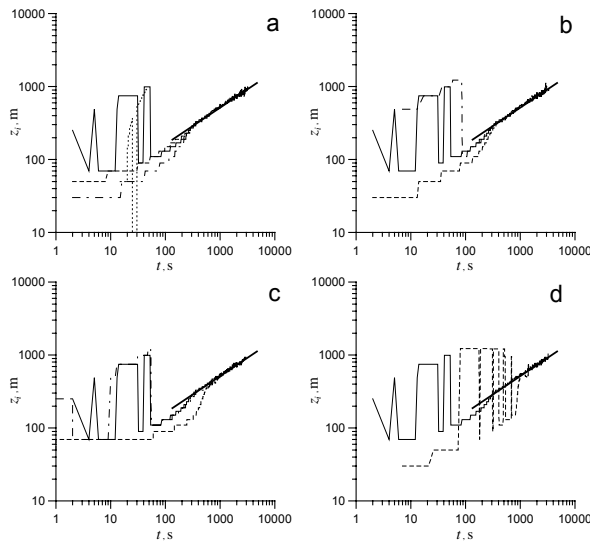


Figure 6. Evolution of inversion height with time for different initiation regimes. See text for notation.

Elevations of the kinematic heat flux minima have been used for evaluation of the CBL depth (inversion height) evolution for selected convection initiation regimes. In Fig. 6, inversion heights for different initiation regimes are shown as functions of time. Solid lines in all plots refer to the NST2W2D case.

In Fig. 6a, the dashed line presents LES results for the analog of the NST2W2D case with the Smagorinsky closure employed instead of the Deardorff closure (it may be called the NST2W2S case). The dashed-dotted line shows LES results with the Smagorinsky closure in the absence of initial temperature perturbations (the NST0W2S case), and the dotted line corresponds to the case with the Smagorinsky closure and zero vertical velocity perturbations (the NST2W0S case).

In Fig. 6b, the dashed line corresponds to the shear-free CBL case simulated with the Deardorff closure and initiated with only vertical velocity disturbances (the NST0W2D case). The dashed-dotted line presents LES data obtained with the Deardorff closure and temperature perturbations only (the NST2W0S case).

In Fig. 6c, the dashed line corresponds to the GCT2W2D case (see above) with strong ( $20\text{m}\cdot\text{s}^{-1}$ ) height-constant geostrophic wind, and the dashed and dotted line refers to the case GST2W2D with geostrophic wind magnitude growing with height from  $0\text{m}\cdot\text{s}^{-1}$  at the surface to  $20\text{m}\cdot\text{s}^{-1}$  at the domain top.

In Fig. 6d, the dashed line corresponds to the shear free CBL case with very small initial perturbations (the NST-W-D case, see Fig. 4).

It should be noted that at the early stages of convection the heat flux minima and associated inversions are usually not well defined. As seen in the Fig. 6, this leads to a large scatter in the  $z_i(t)$  dependencies for particular initiation regimes. The LES with the Smagorinsky closure predicts the CBL growth rather consistently when both temperature and vertical velocity field are initially perturbed. It also works fairly well in the case of solely vertical velocity initial perturbations. However, in the presence of only temperature initial perturbations, the LES with Smagorinsky closure fails to predict the CBL growth correctly.

It is remarkable that  $z_i(t)$  dependencies for all regimes, no matter how much they differ from each other at the early stages of convection, eventually collapse to the same  $1/2$  power dependence that represents a similarity solution for  $z_i(t)$  in the **shear-free** CBL (bold straight lines in Fig. 7). It will be necessary to investigate mechanisms behind such behavior.

**Acknowledgements.** The authors are grateful to Mathieu Pourquie for his essential help in the modification of the employed LES code, and to NSF for the provided funding (grant ATM-0124068).

- Deardorff, J. W., 1980: Stratocumulus-capped mixed layers derived from a three-dimensional model. Convective velocity and temperature scales for the unstable planetary boundary layer and for Raleigh convection. *Bound.-Layer Meteor.*, **18**, 495-527.
- Fedorovich, E., R. Kaiser, M. Rau, and E. Plate, 1996: Wind tunnel study of turbulent flow structure in the convective boundary layer capped by a temperature inversion. *J. Atmos. Sci.*, **53**, 1273-1289.
- Fedorovich, E., F. T. M. Nieuwstadt, and R. Kaiser, 2001: Numerical and laboratory study of horizontally evolving convective boundary layer. Part I: Transition regimes and development of the mixed layer. *J. Atmos. Sci.*, **58**, 70-86.
- Lilly, D. K., 1967: The representation of small-scale turbulence in numerical simulation experiments. *Proceedings, IBM Scientific Computing Symposium on Environmental Sciences*, November 14-16, 1966, Thomas J. Watson Research Center, Yorktown Heights, N.Y., H.H. Goldstein, Ed., IBM Form No. 320-1951, pp. 195-210.
- Nieuwstadt, F. T. M., and R. A. Brost, 1986: Decay of convective turbulence. *J. Atmos. Sci.*, **43**, 532-546.
- Nieuwstadt, F. T. M., P. J. Mason, C.-H. Moeng, and U. Schumann, 1993: Large-eddy simulation of the convective boundary layer: a comparison of four computer codes. *Turbulent Shear Flows 8*, F. Durst et al., Eds. Springer-Verlag, 343-367.
- Rau, M., and E. J. Plate, 1995: Wind tunnel modelling of convective boundary layers. *Wind Climate in Cities*, J. Cermak et al., Eds., Kluwer, 431-456.